Modeling of Forecast Sensitivity on the March of Monsoon Isochrones from Kerala to New Delhi: The First 25 Days

T. N. KRISHNAMURTI, ANU SIMON, AYPE THOMAS, AND AKHILESH MISHRA

Department of Earth, Ocean and Atmospheric Sciences, The Florida State University, Tallahassee, Florida

DEV SIKKA

New Delhi, India

DEV NIYOGI

Department of Earth and Atmospheric Sciences Purdue University, West Lafayette, Indiana

ARINDAM CHAKRABORTY

Centre for Atmosphere, Ocean Studies, IISC, Bangalore, India

LI LI

NRL, Washington, D.C.

(Manuscript received 21 June 2011, in final form 16 November 2011)

ABSTRACT

This study addresses observational and modeling sensitivity on the march of the onset isochrones of the Indian summer monsoon. The first 25 days of the passage of the isochrones of monsoon onset is of great scientific interest. Surface and satellite-based datasets are used for high-resolution modeling of the impact of the motion of the onset isochrones from Kerala to New Delhi. These include the asymmetries across the isochrone such as soil moisture and its temporal variability, moistening of the dry soil to the immediate north of the isochrone by nonconvective anvil rains, and formation of newly forming cloud elements to the immediate north of the isochrone. The region immediately north of the isochrone is shown to carry a spread of buoyancy elements. As these new elements grow, they are continually being steered by the divergent circulations of the parent isochrone to the north and eventually to the northwest. *CloudSat* was extremely useful for identifying the asymmetric cloud structures across the isochrone. In the modeling sensitivity studies, the authors used a mesoscale Advanced Research Weather Research and Forecasting Model (ARW-WRF) to examine days 1–25 of forecasts of the onset isochrone. Prediction experiments were first modeled during normal, dry, and wet Indian monsoons using default values of model parameters. This study was extended to determine the effects of changes in soil moisture and nonconvective rain parameterizations (the parameters suggested by the satellite observations). These sensitivity experiments show that the motion of the isochrones from Kerala to New Delhi are very sensitive to the parameterization of soil moisture and nonconvective anvil rains immediately north of the isochrone.

1. Introduction

The annual cycle of the Asian summer monsoon carries the passage of onset isochrones of precipitation. This is a major feature of the monsoon life cycle. Chang et al. (2004) illustrated the march of the principal monsoonal heat source from Indonesia to the eastern foothills of the Himalayas between January and July and a reverse trek during the remaining months of the year. This is the belt of the heaviest monsoon rains that exhibit an annual seesaw in its traverse pattern. This axis should be labeled as a principal axis of the monsoon. A feature that follows this rain belt is the upper-tropospheric outflow that can

Corresponding author address: T. N. Krishnamurti, Dept. of Earth, Ocean and Atmospheric Science, The Florida State University, Tallahassee, FL 32306.
E-mail: tkrishnamurti@fsu.edu

DOI: 10.1175/JAS-D-11-0170.1

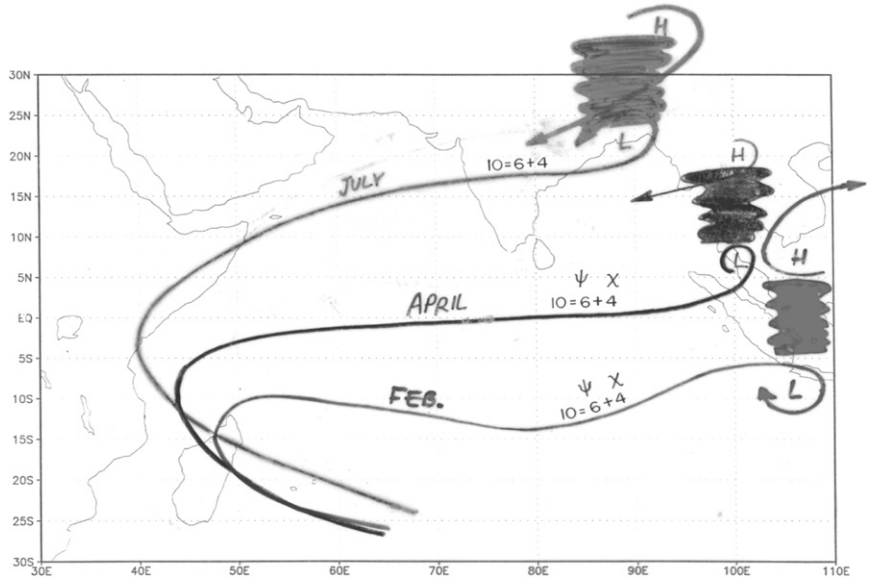

FIG. 1. The northward march of a clockwise flow gyre at 850-hPa level during the months of February, April, and July. This monsoonal low-level flow terminates at the monsoon trough that carries deep convection and clouds, as shown on the right side. Also shown is the upper-tropospheric anticyclonic flow.

be seen as a distinct upper anticyclone such as the Tibetan high. During these months, the flows exhibit a response to the heating, following the symmetric and antisymmetric heating/circulation scenario of Gill (1980). A clockwise large-scale gyre over the Southern Hemisphere Indian Ocean makes its way well into the Northern Hemisphere by July (Fig. 1). This gyre of clockwise circulation meets the southwestern coast of India, the Kerala State, normally during early June. Thus the progress of the broad-scale differential heating also dictates the onset of the monsoon rains over Kerala. The subsequent progress of the onset isochrones is sensitive to the overall structure of heat sources and sinks. The response of the northward progress of the monsoon to the heating along this principal axis of the monsoon was addressed by Krishnamurti and Ramanathan (1982). They noted that flow features such as those during the onset and active monsoon spells were sensitive to the location of the heat source of the monsoon. In that sense, the heating along the principal axis is also important for the isochrone positions. During the months between May and July, these isochrones, plotted at 5-day intervals (Rao 1976), show a passage from the Indian Ocean south of India to the foothills of the Himalayas. The standard deviations of the dates of onset over different parts of India have been summarized by Rao (1976). These isochrones are elongated from the southwest to the northeast and the onset rains shows a meridional and eventual westward motion. Chang (2005) presented a climatology of the onset isochrones for the entire Asian monsoon that looks at the East Asian monsoon and the Indian monsoon in a collective manner (Fig. 2). The Myanmar monsoon onset precedes the Indian monsoon onset by about a month. Lwin (2002) noted that the onset of the Myanmar and Indian monsoon are related to the passage of two successive waves of the intraseasonal oscillation (ISO) that strengthen the Myanmar monsoon westerlies during early May.

Prior to the 1980s there were no formal theories for the meridional propagation of isochrones. Most previous studies were phenomenological. Ananthakrishnan et al. (1968) attributed the meridional motion to the slow seasonal intensification of the monsoon trough that is located near 25°N (i.e., south of the Himalayas). The attendant increase of pressure gradient and frictional convergence resulted in a northward directed lower-tropospheric flow, which they considered an important factor for the northward motion of the isochrones. Yanai et al. (1992) noted a reversal of the tropospheric temperature gradient during the onset of June, indicating that temperature gradient was related to the warming of the air over the Tibetan Plateau, resulting in a warm troposphere to the north and cooler air residing over the equatorial latitudes. Prior to the onset, the air over Tibet is cooler compared with the lower latitudes. With this reversal of temperature gradient, the pressure field behaved in accordance with the findings of Ananthakrishnan et al. (1968) and provided an

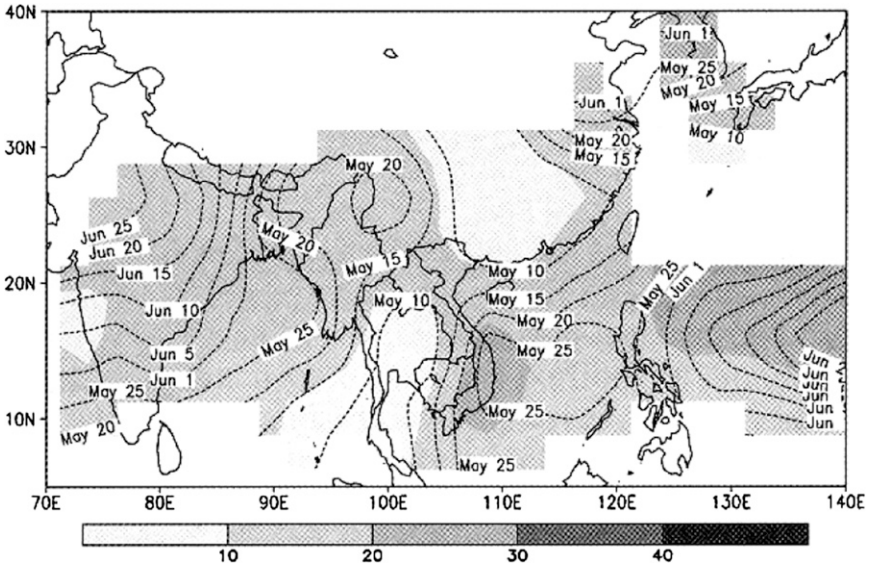

FIG. 2. Climatological isochrones of the onset of the Asian summer monsoon based on the period 1979–99. Shading indicates the standard deviation (days) of the onset date. From Janowiak and Xie (2003).

explanation for the meridional motion of isochrones. In recent years the meridional motion of the isochrones has been related to the meridional passage of the ISO wave. Wang (2005) proposes a theory for the ISO that invokes many factors such as low-frequency equatorial waves, cloud radiation, convective heating, mesosynoptic systems, boundary layer dynamics, air–sea interaction, the oceanic mixed layer, and water vapor variations in his theoretical modeling of the ISO. Basically, these are elements of a comprehensive numerical model that have a role in the meridional propagation of ISO over Asia, according to Wang.

The Kerala onset in India happens during early June from the passage of a second wave of the ISO. Prediction of the passage of the onset isochrones is the same as the prediction of the first rains of the monsoon after a dry season. This does not necessarily convey anything specific about the total rainfall for a season over all of India. From an examination of model output and surface and space-based observations, we noted a scenario that seems to provide an explanation for the meridional motion of the onset isochrones. A typical isochrone during the early part of June is shown in Fig. 3. This illustration is based on the climatological positions of the onset isochrone as defined by the India Meteorological Department (IMD). This line is typically found over the southwestern coast of India, over the Kerala State, and it extends northwestward over the Bay of Bengal coast and passes through the central Bay of Bengal and northward over Bangladesh and the northeastern Indian states. The India Meteorological Department routinely provides valuable annual summaries of the summer monsoon onset (Srivastava and Yadav 2009; Khole et al. 2010, 2011). IMD has adopted the following new objective criteria for declaring monsoon onset over Kerala

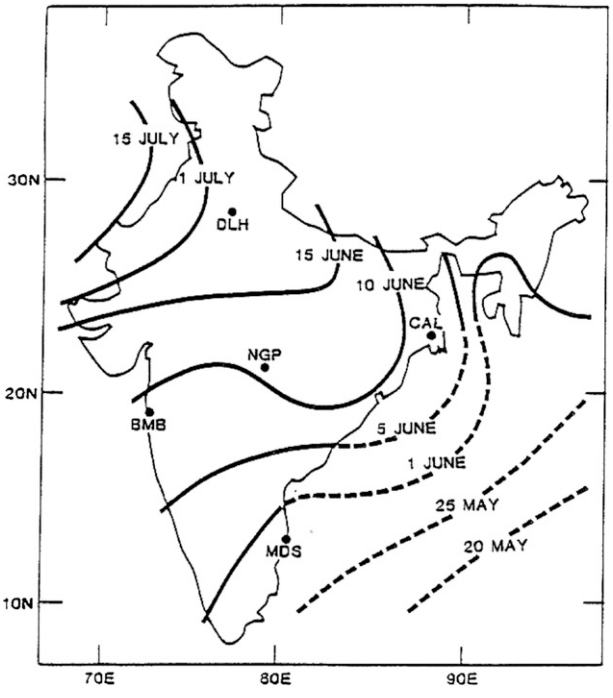

FIG. 3. Climatological positions of the onset isochrones as defined by the India Meteorological Department.

based on rainfall, wind field, and outgoing longwave radiation (OLR) data. The criteria are listed below.

Onset over Kerala is declared on the second day if after 10 May, 60% of the available 14 stations report rainfall of 2.5 mm or more for two consecutive days. The depth of westerlies should also be maintained up to 600 hPa, in the box defined by 0°–10°N and 55°–80°E. The zonal wind speed at 925 hPa over the area bounded by 5°–10°N and 70°–80°E should be at least on the order of 15–20 knots (kt; 8–10 m s^{-1}). Another important criterion is that the Indian National Satellite System (INSAT)-derived OLR value should be below 200 W m^{-2} in the box confined by 5°–10°N and 70°–75°E. After the onset over Kerala, the onset isochrones for the later dates are drawn connecting the places that report rainfall of 2.5 mm or more for two consecutive days.

The landmass to the north and west of this line, not having experienced much rain during the spring season, is close to semiarid. The soil moisture is very low over these land areas with typical values around 0.15 fraction of saturation (volumetric cubic meters of water in 1 m^3 of soil). A couple of days after the passage of the onset isochrone those values jump up to 0.35 of saturation (volumetric cubic meters of water in 1 m^3 of soil). The soil moisture increase generally starts to occur a day or two before the arrival of the onset isochrone. This has to do with a cloud asymmetry across the isochrone. While the clouds over and behind the isochrone carry a larger proportion of deep convective clouds as compared to stratiform clouds, the cloud anvils ahead of the isochrone carry a larger proportion of stratiform rain. The anvils are advected in front of the isochrone by the prevailing divergent circulations. The fresh, lighter rains from the anvils enhance the soil moisture ahead of the isochrones and the warm daytime temperatures facilitate a rapid increase of buoyancy in the region. The enhanced buoyancy results in the growth of newer convective elements ahead of the isochrone. These elements are advected northward and/or northwestward by the prevailing divergent circulation that was produced by the heavy rain of the parent isochrone. As the older clouds undergo their life cycle and die, the newer elements grow and the new isochrone and the entire system shows the familiar isochrone motion from south to north and east to west in the northern latitudes. In certain years, a stagnation of the onset isochrones can be noted possibly related to unusual behavior of the large scale, as reflected by the rotational winds. At times the winds around the Tibetan high can have a stronger northerly component that can contribute to stationarity of the isochrone. This entire scenario is schematically illustrated in Fig. 4. In this paper the observational aspects using conventional datasets and vertical cross sections from *CloudSat*, sensitivity using a mesoscale high-resolution Advanced Research Weather Research and Forecasting Model (ARW-WRF), and validation of this scenario are addressed. The goal of this study is to illustrate the major role of soil moisture, stratiform cloud, and divergent circulations for the motion of the onset isochrones from Kerala at 10°N to New Delhi near 25°N.

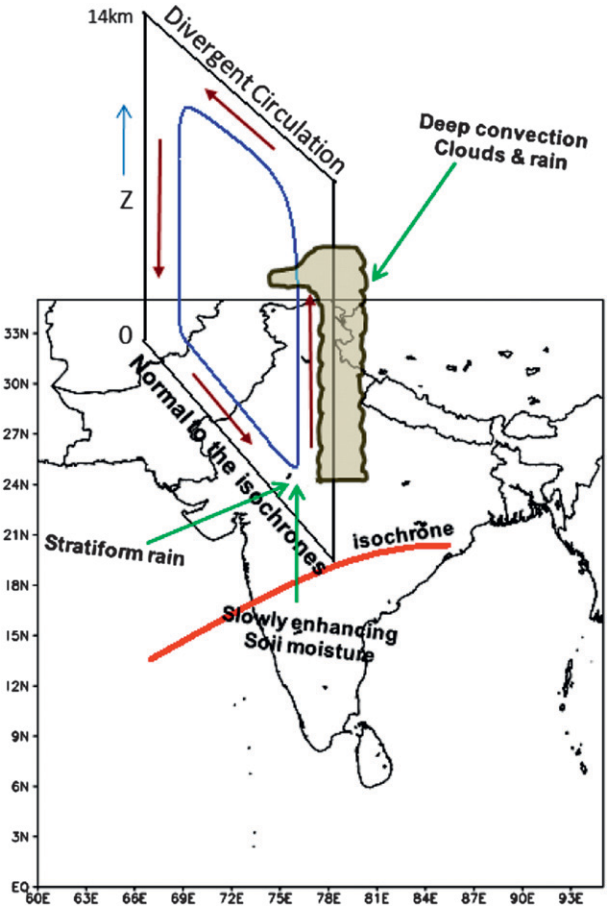

FIG. 4. Schematic of the monsoon onset isochrone, the local divergent circulation, and clouds over the parent isochrone, emphasizing the region immediately forward of the parent isochrone.

2. *CloudSat* imagery across the onset isochrones

CloudSat is a National Aeronautics and Space Administration (NASA) satellite that was launched in 2006. The main instrument is a millimeter-wavelength radar. Ground-based radars generally carry a wavelength of 1 cm. The millimeter-wavelength radar of *CloudSat* enables the detection of much smaller particles of liquid water and ice that define clouds. This cloud radar provides vertical plan views of hydrometeors (the cloud profiling radar). Two other satellites, *Aqua* (provides water vapor profiling), and *Cloud–Aerosol Lidar and*

Infrared Pathfinder Satellite Observations (*CALIPSO*) are important for joint studies with *CloudSat*. Collocated datasets from *CloudSat*, *Aqua*, and *CALIPSO* have enabled NASA to develop algorithms to define cloud structure and type. These datasets are routinely provided by NASA at their website.

Figure 5 carries several *CloudSat* images across the onset isochrone, from the ascending and descending nodes of this satellite. Except for a few pictures of this set, most were from the ascending node (i.e., the satellite was passing from south to north across the landmass of India during the onset month). In these figures, north of the isochrone is marked by the letter "N," and these panels are from different years. It is difficult to show several such images from a single year since the passage of the satellite in any month provides very few such images across the isochrone. The purpose for showing these images is to illustrate the asymmetry of cloud types as we move from the south of the onset isochrone to the north of the isochrone. These pictures include an approximate position of the onset isochrone over India shown by a thick vertical dashed white line; the corresponding date is shown in the top left corner of each panel. These positions are based on our analysis, using the method presented in the appendix. Each date includes two pictures: the top picture for each day is the radar reflectivity cross section and the bottom part carries the cloud types. At the bottom of the two illustrations the color codes for the reflectivity and for the cloud type are provided. The cloud types are determined by a NASA algorithm that looks at the hydrometeors of the *CloudSat* clouds and infers the cloud types statistically. In these images, to the south of the isochrone, the satellite data–based radar reflectivity consistently shows the presence of heavy deep rain clouds of the monsoon. To the north we see mostly two types of clouds, the long anvils of deep convection and developing and somewhat isolated towering cumuli (i.e., convective congestus). This asymmetry is most conspicuous for most of the panels except for one panel dated 9 June 2010 when a plethora of deep convection was also present north of the isochrone. Perhaps the reason for that exception was that several of the developing towering cumuli had grown into taller clouds; even in this instance one can see much larger overall convection behind the marked isochrone. In summary it is possible to see a major asymmetry of clouds across the onset isochrone.

The region to the north of the isochrones is moistened by the anvil rains (nonconvective rains), and the warm surface temperatures and the evaporating rain contribute to a large buoyancy. New cloud elements form and grow in this region ahead of the isochrone. We have examined the asymmetry of clouds across the isochrone for different periods of the monsoon during the last 3 yr and noted very similar structures. This asymmetry is an important characteristic of the newly forming clouds that grow and define a new parent isochrone. The motion of the isochrone seems to be dictated by the divergent circulations described in section 7.

3. Model experiments

a. The ARW-WRF

The ARW-WRF is a collaborative effort among the National Center for Atmospheric Research (NCAR) Mesoscale and Microscale Meteorology Division (MMM) and the National Centers for Environmental Prediction (NCEP) Environmental Modeling Center (EMC). The WRF is a fully compressible, nonhydrostatic model (with a runtime hydrostatic option). Its vertical coordinate is a terrain-following hydrostatic pressure coordinate. The grid staggering is the Arakawa C grid. The model uses the Runge–Kutta second- and third-order time integration schemes, and second- to sixth-order advection schemes in both the horizontal and vertical. It uses a time-split small step for acoustic and gravity wave modes. The dynamics conserves scalar variables. We used the following physics options for this model: Longwave radiation scheme—Rapid Radiative Transfer Model (RRTM) (Mlawer et al. 1997); shortwave radiation scheme—Dudhia scheme (Dudhia 1989; Grell 1993); surface physics—Monin–Obukhov (Janjic) scheme (Monin and Obukhov 1954); land surface model—five-layer thermal diffusion (Skamarock et al. 2005); planetary boundary layer scheme—Mellor–Yamada–Janjic (MYJ) turbulent kinetic energy (TKE) planetary boundary layer (PBL) (Janjic 1994); convection scheme—Kain–Fritsch (new eta) scheme (Kain and Fritsch 1993); and explicit moisture scheme—WRF six-class graupel scheme (WSM6) (Hong and Lim 2006; Hong et al. 2004). The model is run with a single domain at 25-km horizontal resolution and 27 vertical levels.

NCEP's Global Data Assimilation System (GDAS) carries a 6-hourly gridded data archive. The GDAS is derived from the NCEP's operational model runs called the final analysis (FNL). This includes late conventional and satellite datasets (Petersen and Stackpole 1989). This assimilation is run 4 times a day (i.e., at 0000, 0600, 1200, and 1800 UTC). Model output is for the analysis time and a 6-h forecast. Precipitation and surface fluxes are only available at the forecast hours. Details of the GDAS are described by Kanamitsu (1989), Derber et al. (1991), and Parrish and Derber (1992). NCEP postprocessing of GDAS

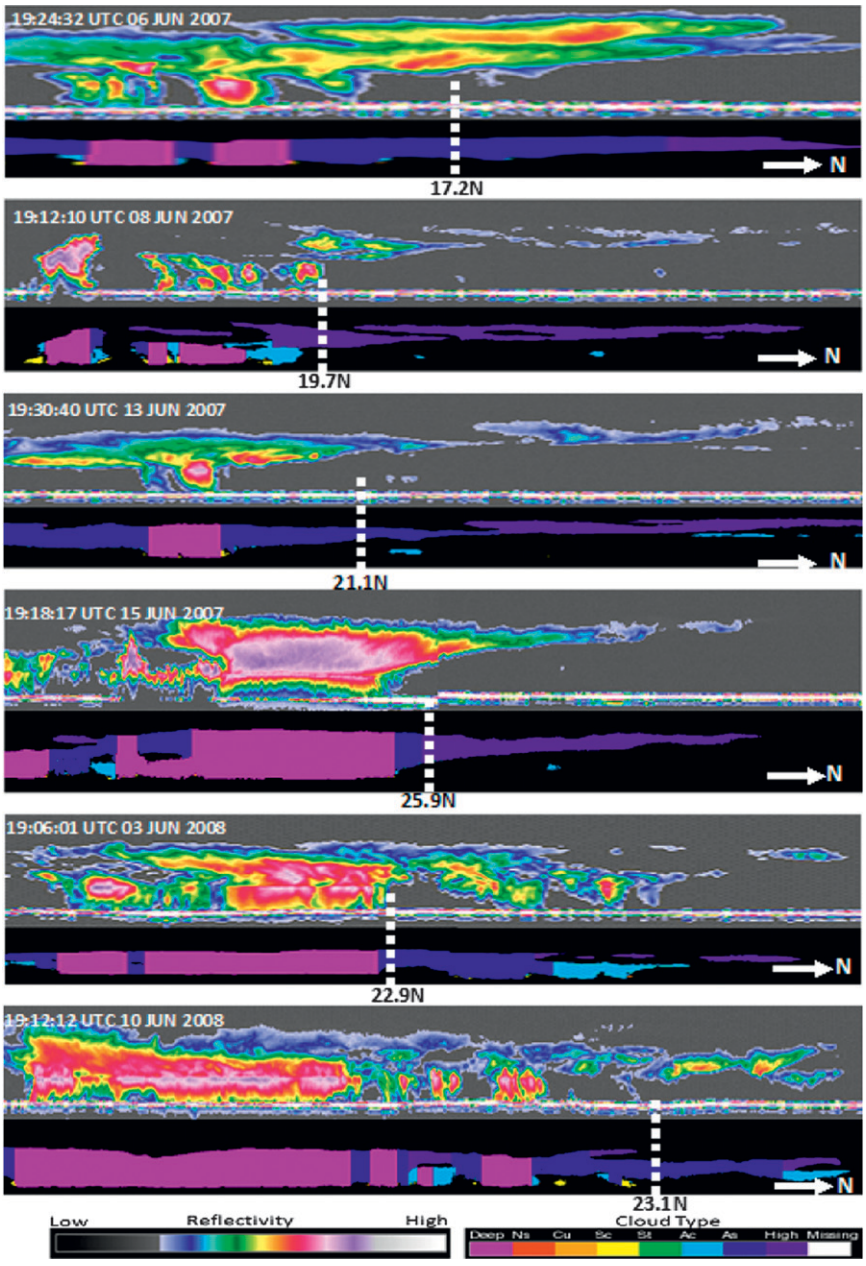

FIG. 5. The IR imagery from the polar-orbiting *CloudSat*, the radar reflectivity implied from *CloudSat*, and cloud types as determined by the *CloudSat* data processing for different days. The vertical dashed line shows the location of the onset isochrone as determined by IMD. The thick arrow marked "N" illustrates the ascending or the descending node of the satellite motion.

converts the data from the spectral coefficient form to 1° latitude–longitude (360 × 181) grids and from sigma levels to mandatory pressure levels. The data in gridded binary (GRIB) format obtained online (from http://rda.ucar.edu/cgi-bin/datasets/dataaccess?dsnum=083.2) are used in our study. The ARW-WRF has an internally built-in bilinear interpolation in space and a linear interpolation in time that uses the large-scale assimilated datasets from the Global Forecast System (GFS) to derive the lateral boundary conditions on the boundaries of the WRF at the resolution of WRF. Those get provided to the WRF at the end of each time step. The lateral boundary conditions are updated every 6 h.

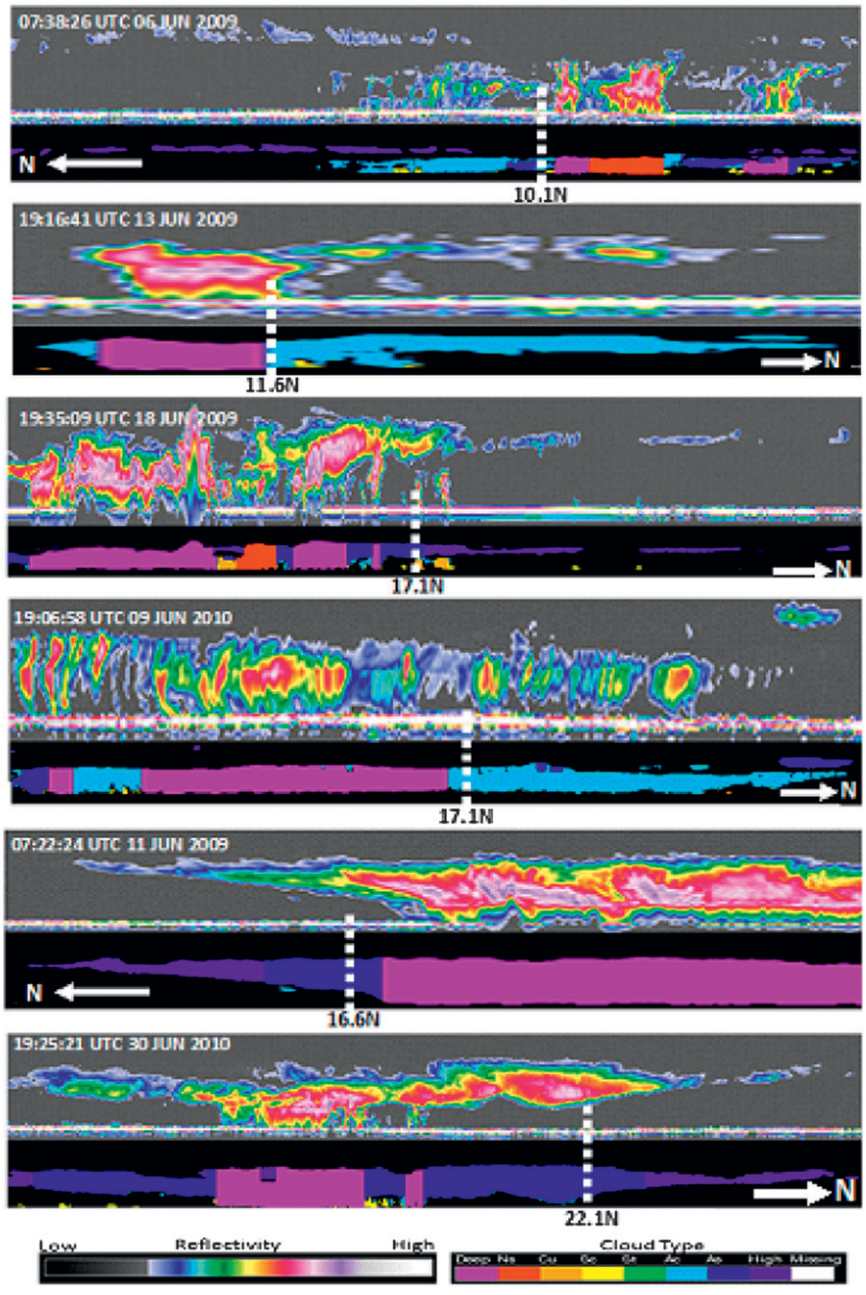

FIG. 5. (*Continued*)

b. The soil moisture parameterization in the ARW-WRF

In most numerical models, the soil moisture algorithm interfaces with the moisture equation of the constant flux layer, thus exchanging precipitation and evaporation relevant to the ground and the atmosphere. The soil moisture algorithm is in fact a time-dependent equation for the forecast of soil moisture over four soil layers that carry thicknesses of 10, 30, 60, and 100 cm. The soil model predicts surface skin temperature, total soil moisture, liquid soil moisture in each layer, soil temperature for each layer, and the canopy water content (this can be dew, frost, or intercepted precipitation). These require initial states that are provided by the WRF Preprocessing System (WPS) of the ARW-WRF based on past experimentation. The soil moisture equation is of the form

$$\frac{\partial S}{\partial t} = \frac{\partial}{\partial z}\left(D\frac{\partial s}{\partial z}\right) + \frac{\partial K}{\partial z} + F_s, \quad (1)$$

where D and K are functions for soil texture and soil moisture, respectively, and F_s represents sources (rainfall) and sinks (evaporation).

The soil temperature prediction equation takes the form

$$C(\theta)\frac{\partial T}{\partial t} = \frac{\partial}{\partial Z}\left[K_t(\theta)\frac{\partial T}{\partial Z}\right], \quad (2)$$

where C and K_t are functions for soil texture and soil moisture. Soil temperature information is used to compute ground heat flux.

The surface water budget is estimated from the relation

$$dS = P - R - E,$$

where dS is the change in soil moisture content, P is precipitation, R is runoff, and E is evaporation.

The evaporation is a function of soil moisture and vegetation type, rooting depth, and the green vegetation cover. This formulation utilizes Noah algorithms of the NCAR models, which also include the parameterizations for surface evaporation, vegetation transpiration, and canopy resistance. These details can be found in Chen et al. (1996, 2001).

In this paper, we began with experiments using the default model from the ARW-WRF. For the sensitivity studies on soil moisture, we altered the soil moisture in various experiments as described below.

c. Nonconvective rain in weather and climate

The definition of nonconvective rain used by radar meteorologists and numerical modelers appears to be somewhat distant from each other. Most numerical modelers invoke nonconvective rain if the location in question carries a dynamic ascent of absolutely stable and near-saturated air. Disposition of supersaturation provides a measure of nonconvective precipitation at that location. Krishnamurti et al. (2006, 167–173) describe two other, more rigorous methods for the estimation of nonconvective precipitation that are variants of this same principle (i.e., the disposition of supersaturation).

The language of the radar meteorologist invokes features such as those shown in Table 1 (Stano et al. 2002). To expect for these two methods to match closely, even after averaging at mesoscale or larger-scale grid sizes, would be difficult to achieve. In most of these radar-based estimates of convective and nonconvective rains, parts of the deep convective systems carry anvils and provide stable nonconvective rains. These are systems where the two coexist in proximity. In large-scale models, mostly in the context of large sheets of stratus and altostratus that span for thousands of miles, in extratropical weather systems, the modeling definition works reasonably well for estimates of nonconvective rain. However, in the monsoon isochrone context, we are dealing with a plethora of deep convection behind, and stratiform anvils ahead of the isochrones. If such coexisting, convective/stratiform cloud systems are important for the motion of the isochrones, then a better definition of stratiform rain may be needed for future modeling. Those can be brought about in cloud-resolving, very high-resolution models, where the microphysical processes are explicitly tagged. In the current ARW-WRF that is presented here, the nonconvective rain at 25-km resolution comes from the disposition of supersaturation. Those results are presented in section 5c. To see further details on the asymmetry of cloud types across the isochrones, a few experiments were also carried out at a 3-km resolution where explicit clouds, instead of parameterized clouds, were used. Those structures are described in section 6.

TABLE 1. Criteria for determining convective and stratiform rain as seen by TRMM radar.

Condition	Convective rain	Stratiform rain
Presence of light bands		✓
Absence of bright bands	✓	
Reflectivity 20–40 dBZ	✓	✓
Reflectivity > 40 dBZ	✓	
Presence of strong gradients of radar reflectivity	✓	
Absence of reflectivity gradients and reflectivity > 20 dBZ		✓

4. Results from modeling

a. A control experiment during a near-normal rainfall year

We selected the monsoon of the year 2000 for the control experiment since the model-based rainfall totals for the first 25 days, all India averaged, were close to the observed totals for the same period. In Fig. 6 we show, by a dark line, the observed march of the isochrones for the summer monsoon of the year 2000. This is based on an official IMD product. The predicted field of the onset isochrones from the mesoscale ARW-WRF is shown as

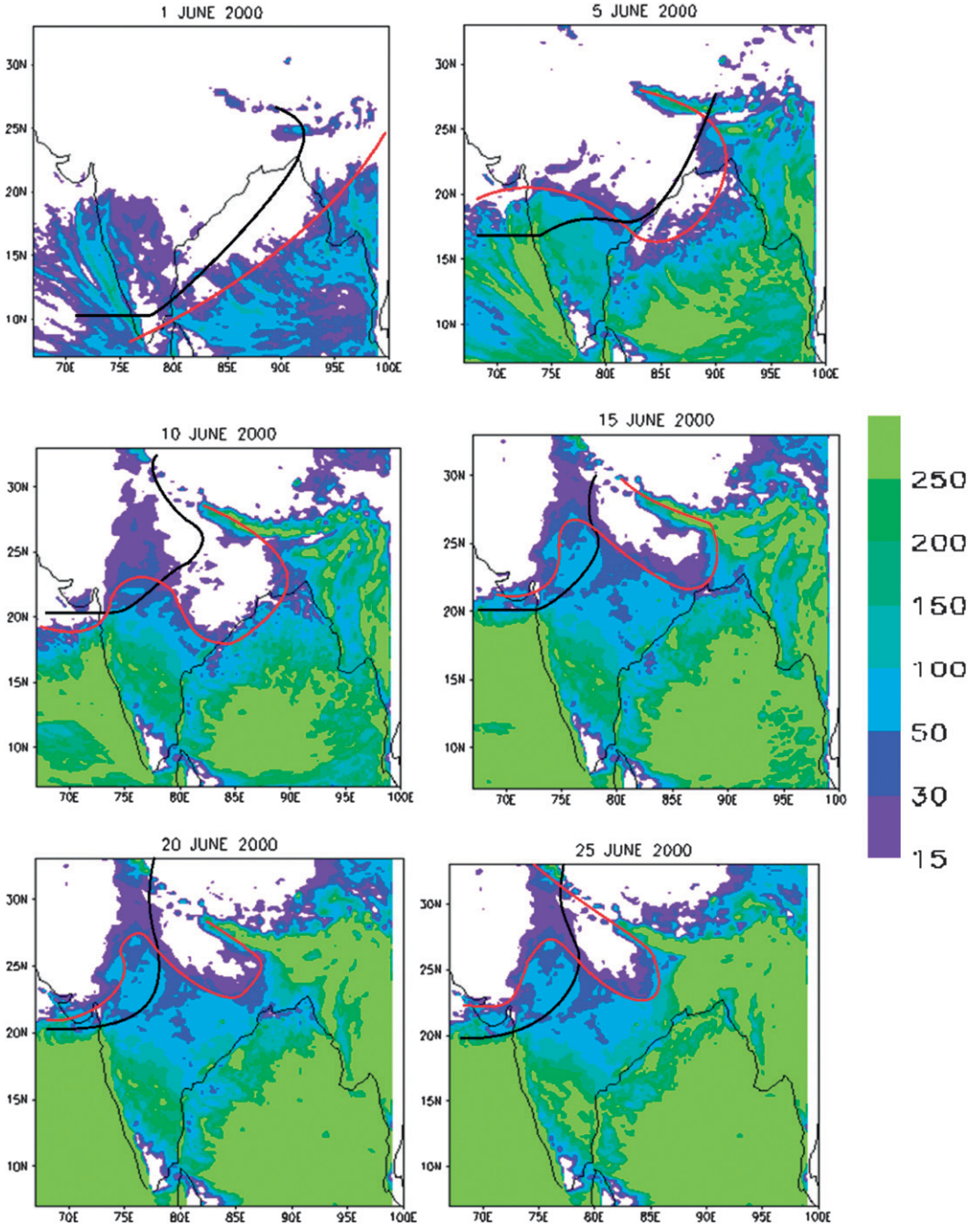

FIG. 6. Accumulated precipitation (mm) for the year 2000. The IMD onset isochrone is marked as a black line and the predicted is marked in red.

a red line in Fig. 6. Here the accumulated precipitation is also shown in each panel, where the panels cover the dates 1–25 June at an interval of roughly 5 days. The forecast has many deficiencies, including the initial position of the isochrone, observed versus modeled discrepancies, and an almost 3° latitude displacement over the Bay of Bengal. Forecasts generally improved during the first 5 days, and the day-5 forecast showed the least errors and thereafter the model isopleth motion was consistently slower compared with the observed positions. Such errors have to be expected because the current predictability for tropical rainfall prediction is only on the order of a few days. Through sensitivity studies, shown in the next section, the goal is to find out factors

that can either slow down or speed up the motion of the isochrones. This, as well as two other examples presented below, is shown to illustrate the nature of the current prediction using a ARW-WRF that utilized some default values for various parameters. Overall this is not a very poor forecast for day 25, considering that a northwestward march of the isochrone is implied by this forecast with overall errors that are less than 4° of latitude.

b. *Modeling isochrone motion during a dry monsoon year*

The observed isochrones for the 2002 season, based on the IMD datasets, are shown in Fig. 7 by a dark line. This was a below-normal monsoon rainfall year. The march of the isochrones during the first 25 days reflected a slower-than-normal meridional motion. The accumulated predicted rains preceding the forecast day, in color shading, are shown at intervals of 5 days, and the predicted isochrones are shown by a red line (Fig. 7). The model, in general, carries a somewhat slower northward and eventual northwestward motion for the isochrone; as a result, the control run of the model predicted a somewhat drier monsoon compared to the dry season of 2002. Overall, again this was a very reasonable forecast for the positioning of the isochrone through day 25 of the forecast, since the position errors were less than 5° in latitude. The message conveyed by this analysis for the years 2000 and 2002 is that there is considerable variability in the rate of meridional motion of the onset isochrones from Kerala to New Delhi in different years. This is a topic of considerable interest from the perspective of interannual variability and the model sensitivities presented in this study.

c. *Modeling isochrone motion during a wet monsoon year*

This was the 2003 summer monsoon: the seasonal totals of rain over all of India were above normal, but the onset of monsoon over Kerala, on the southwestern coast of India, was delayed by a week. Figure 8a illustrates the march of isochrones as seen from observations. The Global Precipitation Climatology Project (GPCP) precipitation is used here. The observed and predicted isochrones for this experiment are shown in Fig. 8b. Also shown are accumulated rainfall totals proceeding the day for which the forecast is labeled. This was again a fairly reasonable forecast for the march of the isochrone during the first 25 days of forecast. As in all previous experiments, the motion of the predicted isochrone was roughly 3°–4° latitude slower than the observed positions. Clearly, model improvement is needed to somewhat speed up the motion of the isochrone. This is addressed in the next section.

5. Sensitivity studies

Observations and modeling suggest that two parameters, the parameterizations of nonconvective rain and the representation of soil moisture, have a strong impact on the meridional motion of the monsoon onset isochrones. These are illustrated in this section.

a. *Variations of soil moisture and precipitation across the isochrones*

The asymmetry of soil moisture across the onset isochrone can be displayed from the soil moisture datasets from the WindSat instrument aboard the U.S. Navy satellite *Coriolis*. WindSat is a satellite-based polarimetric microwave radiometer developed by the Naval Research Laboratory Remote Sensing Division and the Naval Center for Space Technology for the U.S. Navy and the National Polar-Orbiting Operational Environmental Satellite System (NPOESS) Integrated Program Office (IPO) (Li et al. 2009). To show the asymmetry of soil moisture across the onset isochrone we had to composite 3 yr (2009, 2010, and 2011) of datasets. The composited results are shown in Fig. 9a. Here the abscissa denotes the distance ahead of the isochrone, and the ordinate shows soil moisture and rainfall (mm day^{-1}). The compositing method is nontrivial. Each individual isochrone image was processed such that the distance forward or aft of the nearest point of the isochrone on the second day was computed for each pixel (this is based on pixel level data), on which WindSat retrievals are next performed. For consistency the Tropical Rainfall Measuring Mission (TRMM) rainfall datasets were also examined at the pixel level. Although pixel-level datasets were used, compositing was only possible at a resolution of 100 km because sufficient data at the pixel resolution were not available to a finescale compositing. The message conveyed by this compositing is that when the isochrone is moving (north or northwest) the soil moisture carries a low value of around 0.07 well north of the isochrone at distances on the order of 500 km or larger. However, the important finding here is that a sharp increase of soil moisture is noted through roughly a distance of 150 km to the north of the isochrone (where the soil moisture is around 0.07). At the location of the isochrone the soil moisture difference carries values as high as 0.126. This region to the immediate north of the isochrone (from the isochrone to a distance 150 km to the north) experiences rainfall rates on the order of 7 mm day^{-1}. Both datasets for the soil moisture and the precipitation show

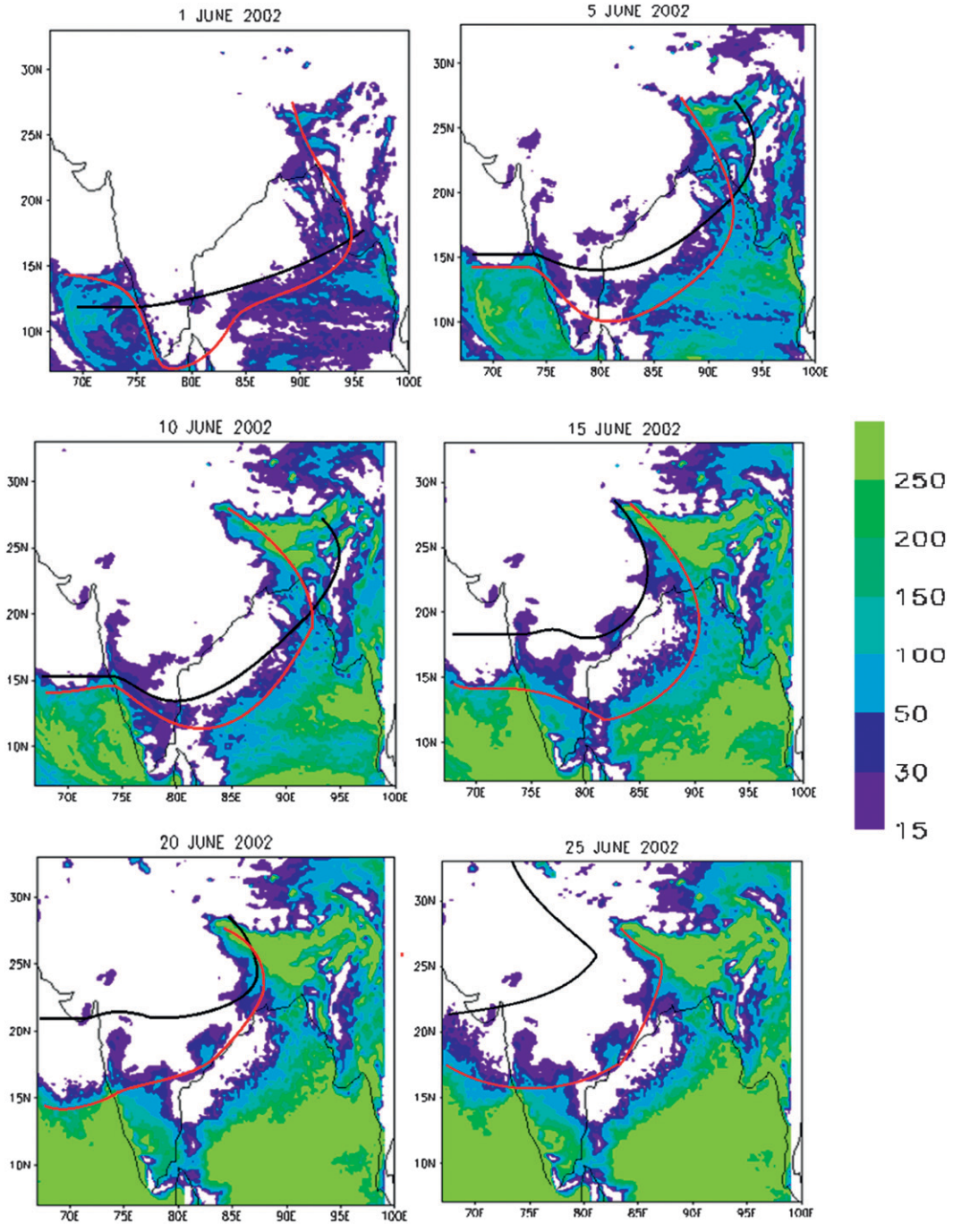

FIG. 7. Accumulated precipitation (mm) for the year 2002. The IMD onset isochrone is marked as a black line and the predicted is marked in red.

that they do not tail off to very low values immediately to the north of the onset isochrone.

Figures 9b and 9c show the time variations of the predicted soil moisture (right ordinate) and of the predicted precipitation (left ordinate) at two single grid points during the passage of the isochrone. The abscissa shows the latitude normal to the isochrone with respect to a specific location of the passage of the isochrone. The dataset is simply obtained from model outputs during a forecast for the June 2000 onset. The location of the isochrone is marked by an arrow. Both the precipitation and the soil moisture show a drop in values north of the isochrone.

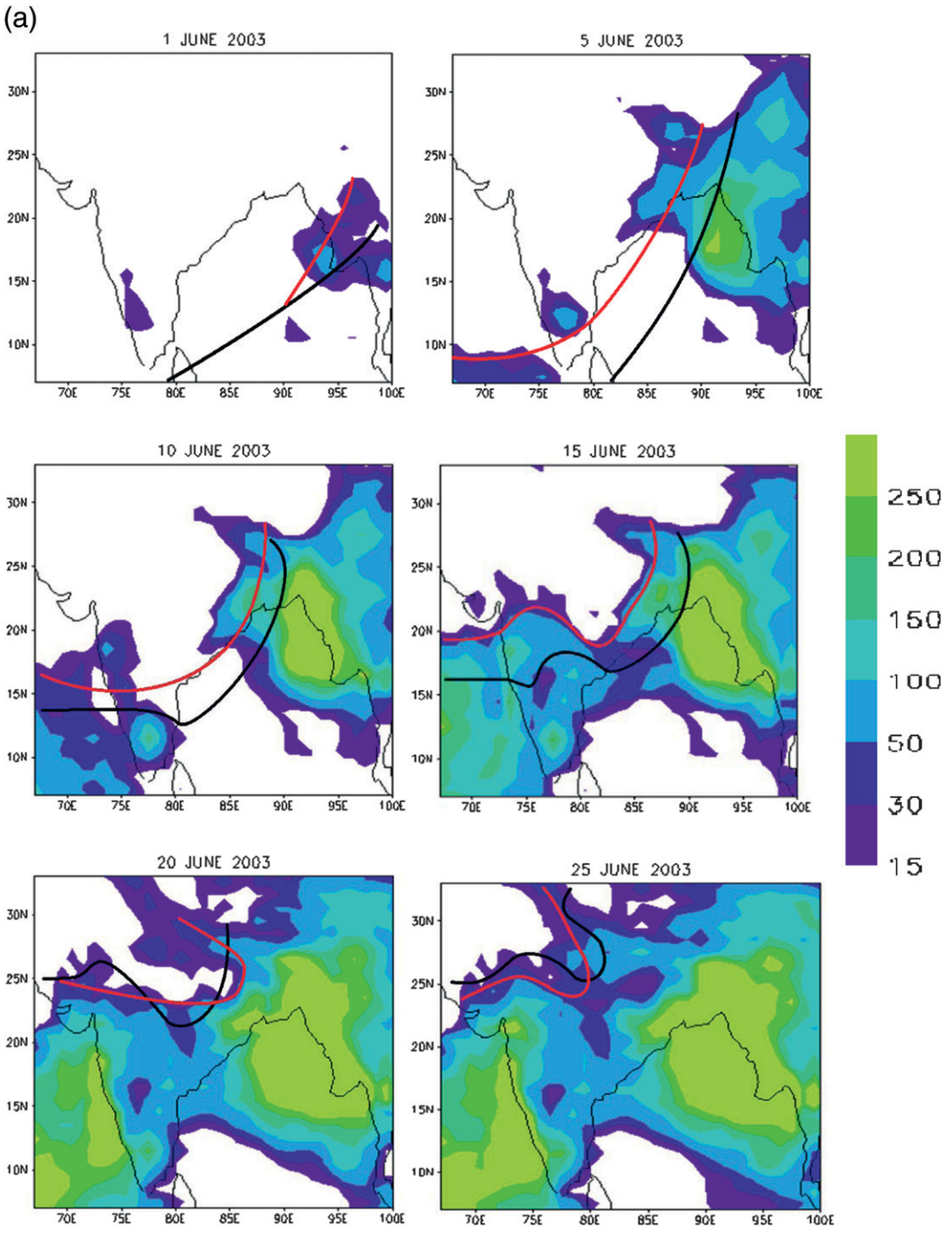

FIG. 8. (a) Accumulated precipitation (mm) for the year 2003 from the GPCP rainfall observations. The IMD onset isochrone is marked as a black line and the predicted line is marked in red. (b) Accumulated precipitation (mm) for the year 2003 from the current experiment. The IMD onset isochrone is marked as a black line and the predicted is marked in red.

This region to the north of the isochrone does not have a very sharp drop in precipitation because of the presence of newly growing cloud elements and the anvil rain. This is also reflected in the slower drop of values of the soil moisture as one proceeds north of the isochrones. Precipitation and soil moisture ahead of the isochrone contribute to increased buoyancy over this region immediately ahead of the isochrone where newer clouds can grow. Typical distributions of buoyancy are illustrated in section 6.

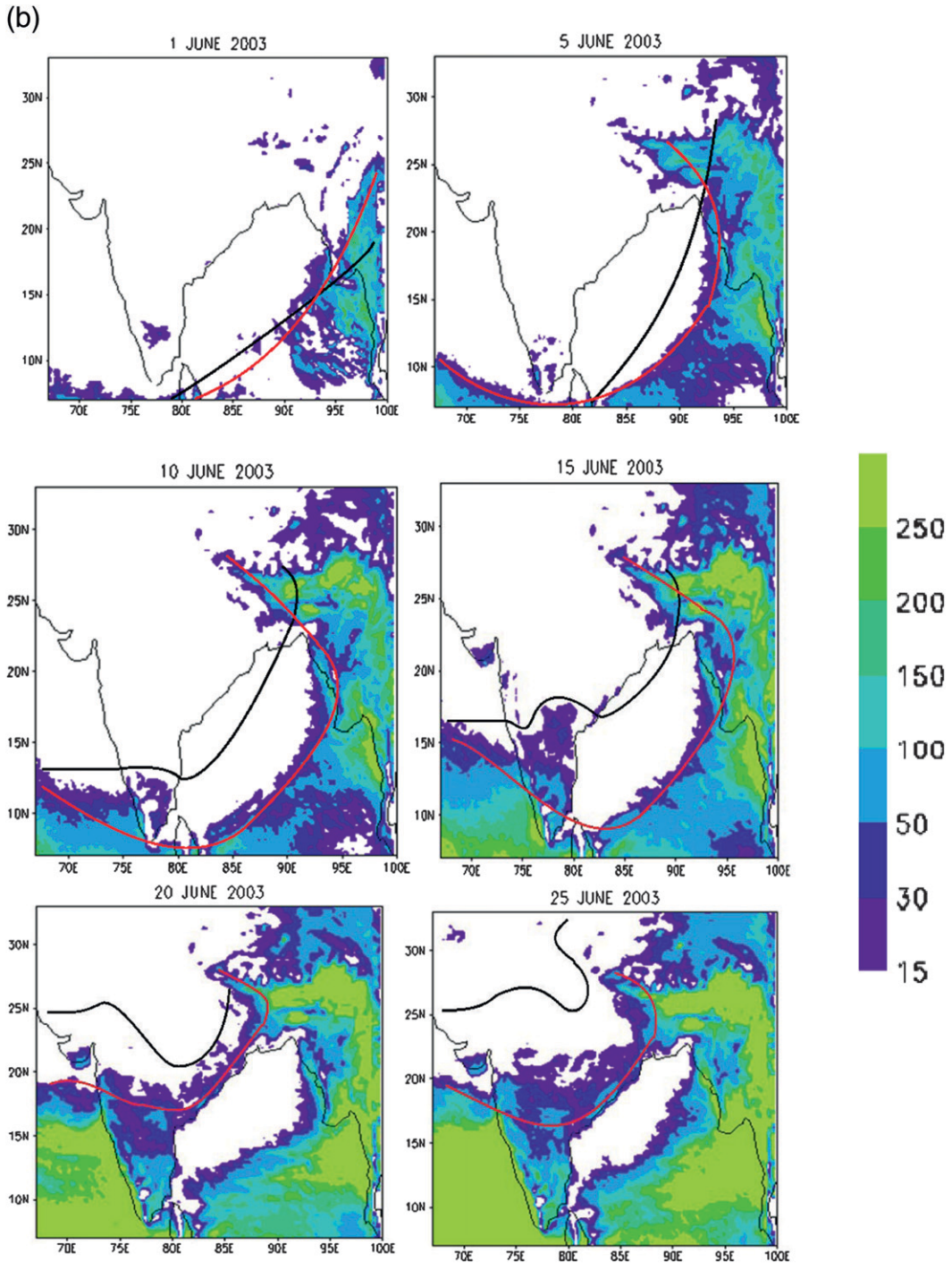

FIG. 8. (*Continued*)

b. Enhancing soil moisture by 15% over the entire land area of the domain

In section 3b, the current soil moisture scheme was described and was always used as a default scheme. The results from that scheme were presented in Fig. 8. After some trial and error, it was noted that a uniform 15% increase in the overall soil moisture compared to what the ARW-WRF provides would reduce the error in the rate of meridional propagation of the isochrones. At each time step after the rainfall (from the model) is computed, the grid soil moisture was modified by 15%,

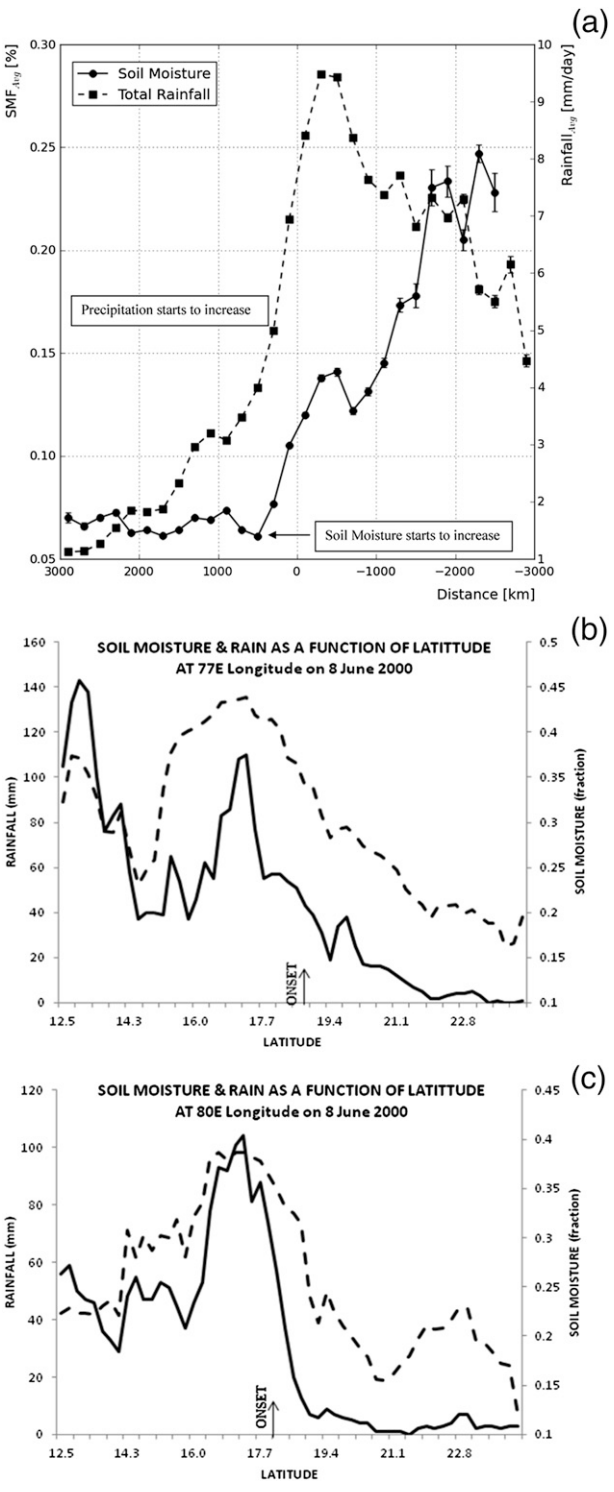

FIG. 9. (a) The variation of soil moisture and rainfall as a function of distance from the isochrone. Soil moisture (fraction) is plotted as a solid line and rain (mm day^{-1}) as a dashed line. The soil moisture data is taken from the instrument WindSat aboard U.S. Navy satellite *Coriolis* and rainfall is from TRMM; these are both based on pixel level measurements. (b),(c) The variation of soil moisture (fraction) and rain (mm day^{-1}) as a function of latitude. These graphs were taken from model output on 8 June 2000 at two grid points that experienced a passage of the onset isochrone. The location of the onset isochrone is marked.

depending on whether a particular grid point has rainfall. In experiment 1, the soil moisture is increased uniformly 15% at all grid points, and in experiment 2, the soil moisture is increased by 15% at five grid locations north of the raining grid. Only the soil moisture at the top layer is modified. As always, ocean points carry a tag of 0.9 and above and those were left alone. Those results for the 2003 season are presented in Fig. 10. Here a much closer agreement between the model-predicted positions of the isochrones and the observed positions as noted by IMD for all map times are noted. The errors in the positioning of the isochrone for most panels are on the order of 2° latitude. This is a very promising result. Such an overall enhancement of soil moisture is, however, not necessary, since the motion of the isochrone is most likely affected by what goes on in its immediate vicinity. Our contention, based on observations, is that the region to the immediate north of the isochrone was most important in this regard. Here the enhanced soil moisture contributes to enhanced evaporation over a previously very dry and hot region. That evaporation contributes to formation of new clouds and enhanced buoyancy over this region to the north of the isochrone, thus permitting further growth and a slow formation of a new position for the isochrone. The isochrone itself moves north and eventually northwestward because of the orientation of the divergent wind that steers these newly forming elements. The next experiment shows results from an enhancement of soil moisture to immediately north of the isochrone.

c. *Enhancing soil moisture to the immediate north of the isochrone*

Since what must influence the northward motion of the isochrone is the soil moisture to the immediate north of the isochrone, a simple experiment was designed. Here we increased the soil moisture perpendicular to the leading edge of the isochrone over five successive grid points by 15% compared to the default values of the ARW-WRF discussed in section 4. The 15% value came from some experimentation that basically yielded almost the same results as shown in the previous section where the soil moisture was enhanced by 15% over the entire land area of the computational domain. These new results are presented in Fig. 11. This confirms the idea that the isochrone motion is largely sensitive to the

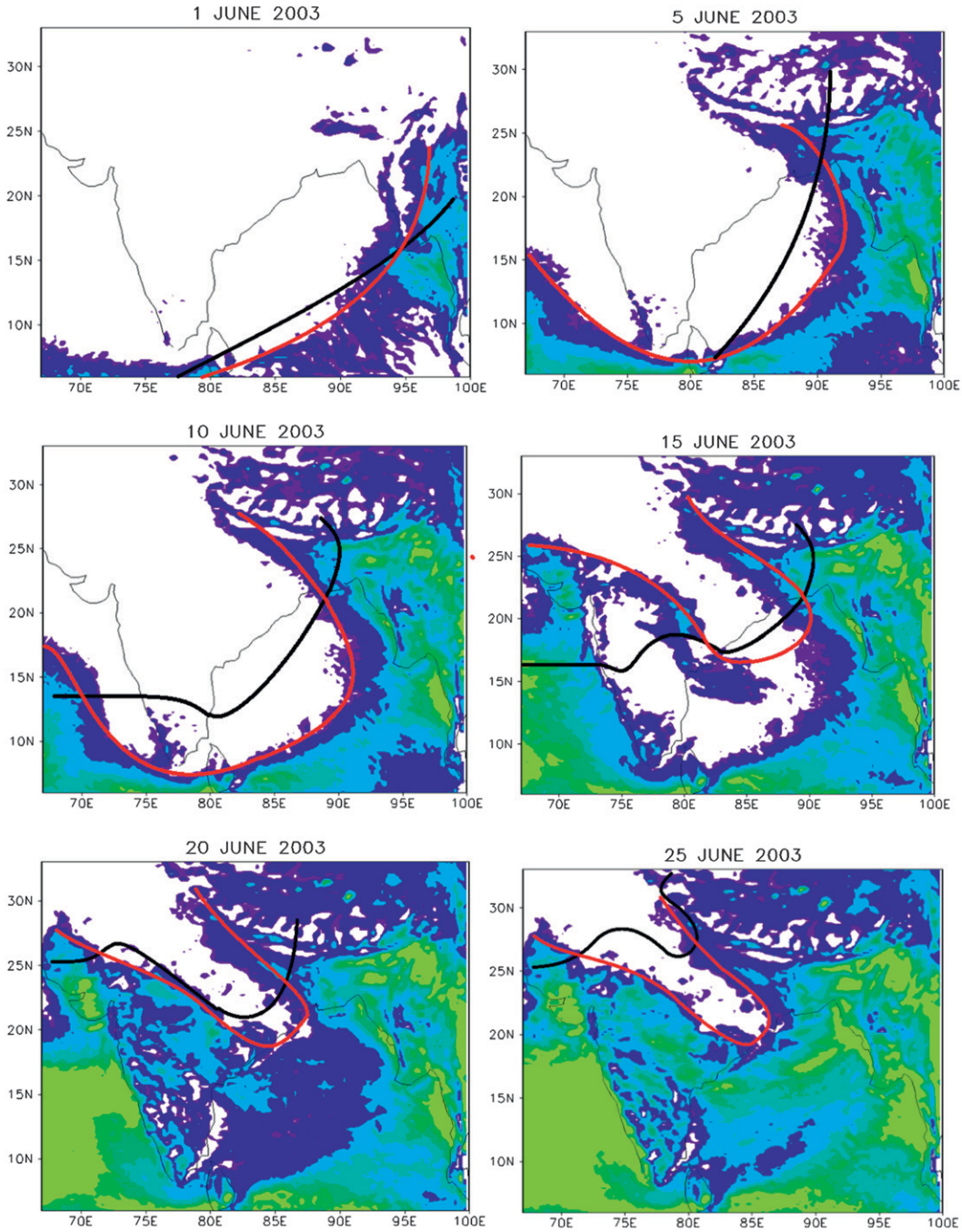

FIG. 10. Accumulated precipitation (mm) for the year 2003 from the ARW-WRF sensitivity experiment of enhancing soil moisture by 15% over the entire land area. The IMD onset isochrone is marked as a black line and the predicted is marked in red.

soil moisture to the immediate forward side of the isochrone. This is the region where anvil and newly forming towering cumuli carry some rain and contribute to an enhancement of the soil moisture. It should be noted that when the soil moisture was changed over the land area, the overall positioning of the onset rains and the placement of the isochrone were altered by the model over land. Those altered winds in the low levels seem to affect the position of the isochrone over the neighboring oceans as well. In Fig. 11a the big differences over the ocean between the control experiment and the modified soil moisture experiment emerged after 2 days. It should be noted that landmasses are present on both sides of the ocean and the soil moisture is modified over Myanmar area also.

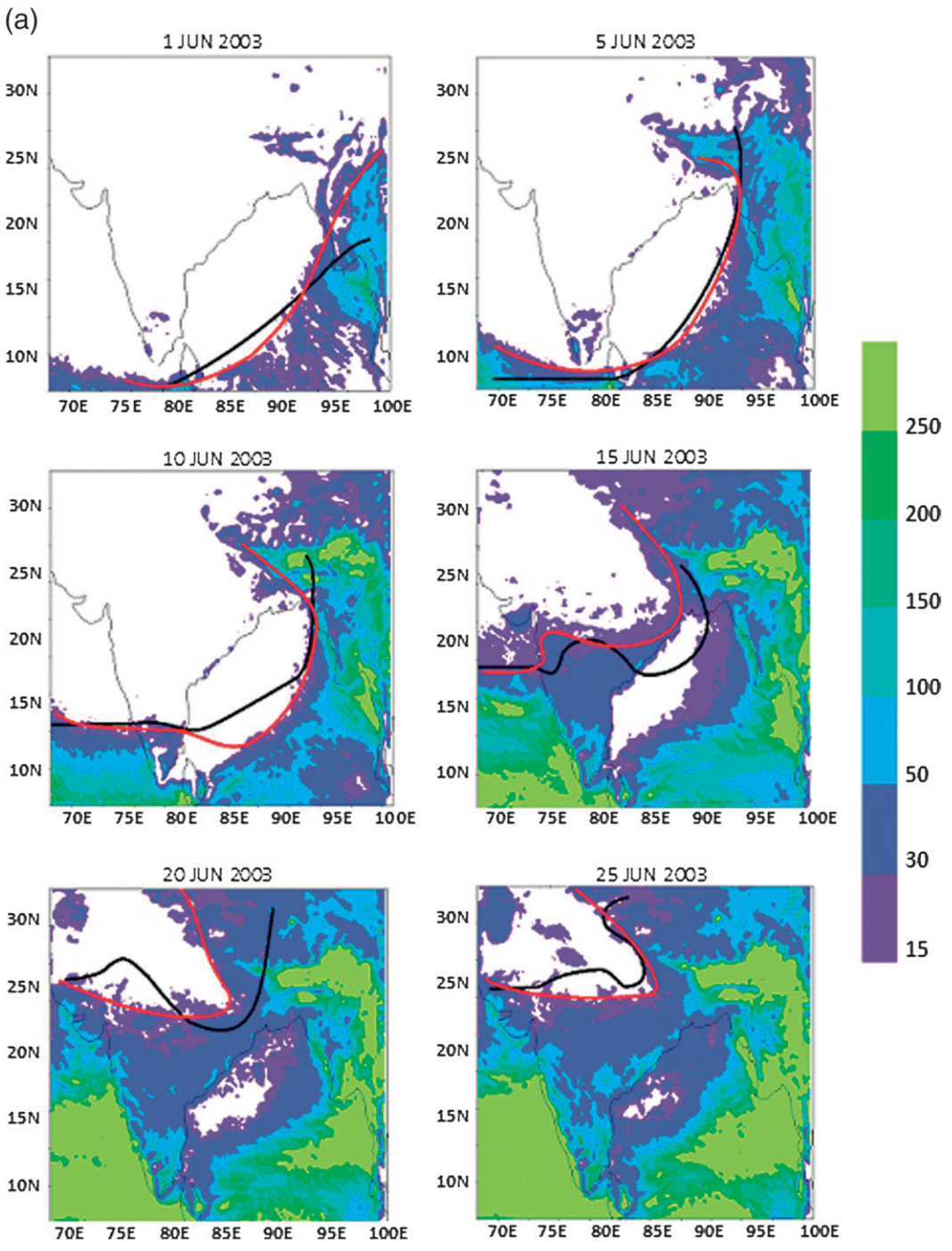

FIG. 11. (a) Accumulated precipitation (mm) for the year 2003 from the ARW-WRF sensitivity experiment of enhancing soil moisture by 15% ahead of the onset isochrone. The IMD onset isochrone is marked as a black line and the predicted is marked in red. (b) Accumulated precipitation (mm) for the year 2003 from the ARW-WRF sensitivity experiment of enhancing stratiform rain by 15% ahead of the onset isochrone. The IMD onset isochrone is marked as a black line and the predicted is marked in red.

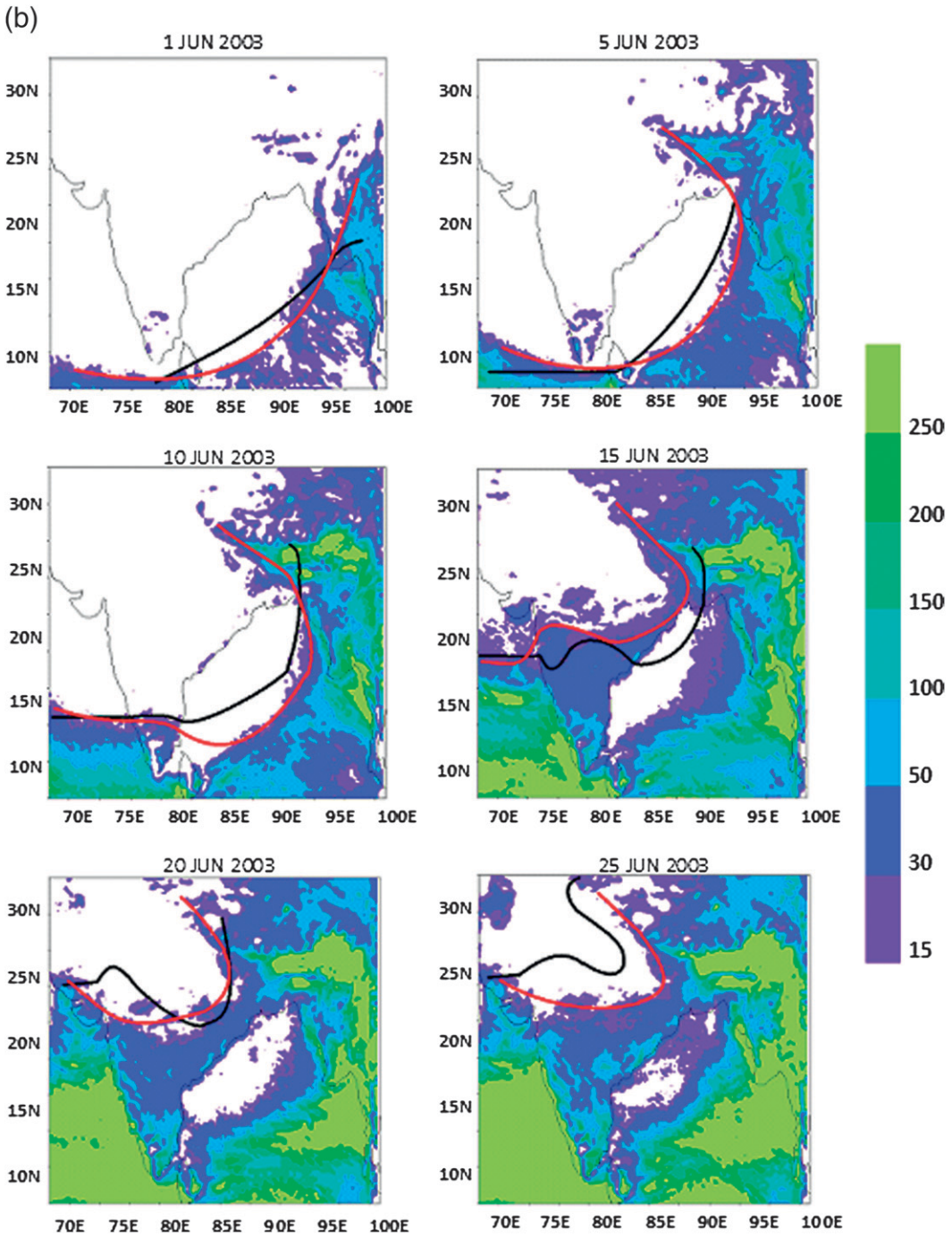

FIG. 11. (*Continued*)

d. Sensitivity experiment for the enhancement of nonconvective rain

Through experimentation, a large sensitivity was noted for the speed of motion of the isochrones of monsoon onset to the parameterization of nonconvective rain discussed in section 3c. The disposition of supersaturation asks for a model relative humidity of 100%. Since this is a stringent requirement because there may be some subgrid-scale regions of subsaturation, that threshold value has been reduced in most operational modeling. After some experimentation, it was noted that a value of around 85% was better suited for anvil rains. The anvil rains occur from pressure levels below 400 hPa. Here the

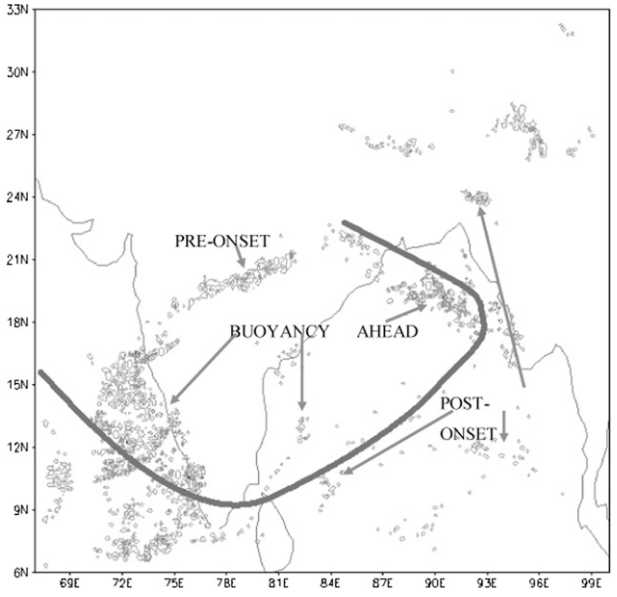

FIG. 12. The buoyancy distribution (m s^{-2}) from the mesoscale forecast for 15 June 2003. This is day 14 of the forecast. The predicted location of the isochrone is shown by thick line. Also identified are some features of the buoyancy distribution with respect to the predicted isochrone.

criteria for the ascent of absolutely stable and saturated air are met for invoking nonconvective rain. It was further noted that even that threshold did not adequately cover the needed enhancement of soil moisture. This led to experimentation in which the nonconvective rain ahead of the leading edge of the isochrone was enhanced successively by 10%, 15%, and 35%. This enhancement was necessary to account for subgrid-scale regions of possible saturation. The best results (Fig. 11b) came from enhancing subgrid-scale rains by 15% where the observed and the predicted isochrones carried an error in positioning by 2° latitude or less during the 25-day forecast.

6. The buoyancy field ahead of the leading edge of the isochrone

The buoyancy is defined as follows:

$$B = g\left(\frac{T'_v}{\overline{T_v}} - r_l\right), \tag{3}$$

where r_l is the liquid water mixing ratio, and T'_v and $\overline{T_v}$ respectively denote virtual temperature values inside a cloud (where $r_l > 0.1$ g kg^{-1}) and outside a cloud (where $r_l < 0.1$ g kg^{-1}). Also, T_v is the virtual temperature and is defined as

$$T_v = 1 + (r_v/\varepsilon)/(1 + r_v)T,$$

where T denotes air temperature, r_v is the mixing ratio of water vapor, and ε is the ratio of molecular weights of water vapor and dry air ($\varepsilon = 0.622$).

To illustrate the details of the isochrones' evolution, we have repeated several of the experiments, presented here, at a 3-km resolution. That is particularly useful for seeing the region ahead of the leading edge of the isochrone. Figure 12 illustrates a typical field of the buoyancy from the model output field. This makes use of the predicted liquid water mixing ratio. This shows several interesting features including a spread of buoyancy ahead of the leading edge of the isochrones. This is the region where the buoyancy helps the growth of a new line of clouds, thus establishing new isochrones in place of the older isochrones. We also see a distribution of positive buoyancy behind the isochrones where the monsoon becomes active subsequently. Also seen in the illustration were some premonsoon onset thunderstorm regions that showed a line of positive buoyancy.

Radar reflectivity cross section across the predicted isochrones

Figure 13 shows a vertical cross section, computed inversely, from the model-predicted hydrometeors. This is a standard output product that is included for all high-resolution forecasts of the ARW-WRF. This model forecast was made at a horizontal resolution of 3 km. In this figure, the ordinate is a height coordinate and the abscissa denotes longitudes across the isochrone for 15 June 2003. Here we are portraying an isochrone that was located over northeastern India and the forward side of the isochrones is to its west. This was the forecast for day 14; the left half of the diagram denotes the front side of the isochrone and the right half denotes the back side of the isochrone. Of interest here are the radar reflectivities to the forward side that carry some upper clouds and weaker deep convective elements. Those are important features that were noted in the *CloudSat* imagery of the radar reflectivity, as shown in Fig. 5c.

7. Local divergent circulations and the onset isochrones' passage

Given the mesoscale model forecasts on the passage of onset isochrones, the postprocessing of local divergent circulations gives an important perspective for the passage of these isochrones. The divergent circulations roughly emanate from regions of the largest vertical upward motions and heavy rains. This divergent circulation steers the newly forming precipitating elements that lie ahead of the isochrones in a direction that is roughly perpendicular to the line of heavy rains. The mapping of those features from the model output is

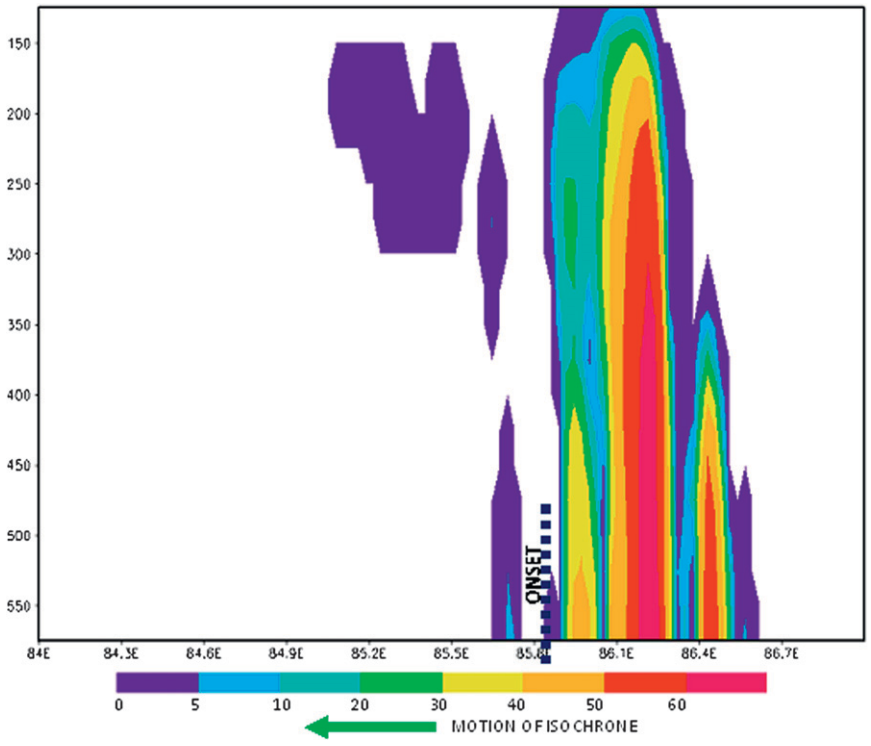

FIG. 13. The model-based radar reflectivity cross section across the isochrone for 15 Jun 2003. The ordinate is height and the abscissa shows longitude normal to the isochrone. Here the left side is the front side of the isochrone and the right side is to the back side of the isochrone. The lower cloud reflectivity values, ahead of the isochrone, are the important feature here.

illustrated in this section. The divergent circulations are computed from the following equations:

$$\nabla^2\chi = -\left(\frac{du}{dx} + \frac{dv}{dy}\right). \tag{4}$$

Given the horizontal velocity components u and v, one can compute the velocity potential χ by solving the above Poisson equation (Krishnamurti and Bounoua 1996, 259–266). The divergent wind is given by the relations

$$U_\chi = -\frac{\partial\chi}{\partial X}, \tag{5}$$

$$V_\chi = -\frac{\partial\chi}{\partial Y}. \tag{6}$$

Those divergent wind components were computed, at the 200-hPa level, to show the steering for the newly formed precipitating cloud elements ahead of the parent clouds of the isochrone. In Fig. 14a, the divergent winds from the FNL analysis are illustrated on top of the velocity potential χ of the 200-hPa surface. These results pertain to 15 June 2003. The weakness ahead of the isochrone lie in a region that carries strong divergent wind steering directed away from the isochrone. The isochrone is strongly dictated by the steering of newly growing deep convection ahead of the parent isochrone. The rotational part of the wind, Fig. 14b, is nearly always parallel to the isochrone, and that stronger wind does not steer the isochrone. The divergent wind is perpendicular to the isochrone in its vicinity and is better able to steer the newly growing precipitating cloud elements. As these new elements grow and the older elements of the isochrone die, a new position of the isochrone is established. Figure 14c shows the predicted 200-hPa level velocity potential and the divergent wind streamlines. This applies for day 15 of the forecast valid on 15 June 2003. These are the results from the mesoscale model forecast from the ARW-WRF. The salient observed features of the divergent wind can be seen here. The model forecast carries a divergent flow that provides the northward steering for the newly forming cloud line that replaces the preceding isochrone.

8. Summary

This study addresses the meridional march of the summer monsoon onset isochrones. Here we examine

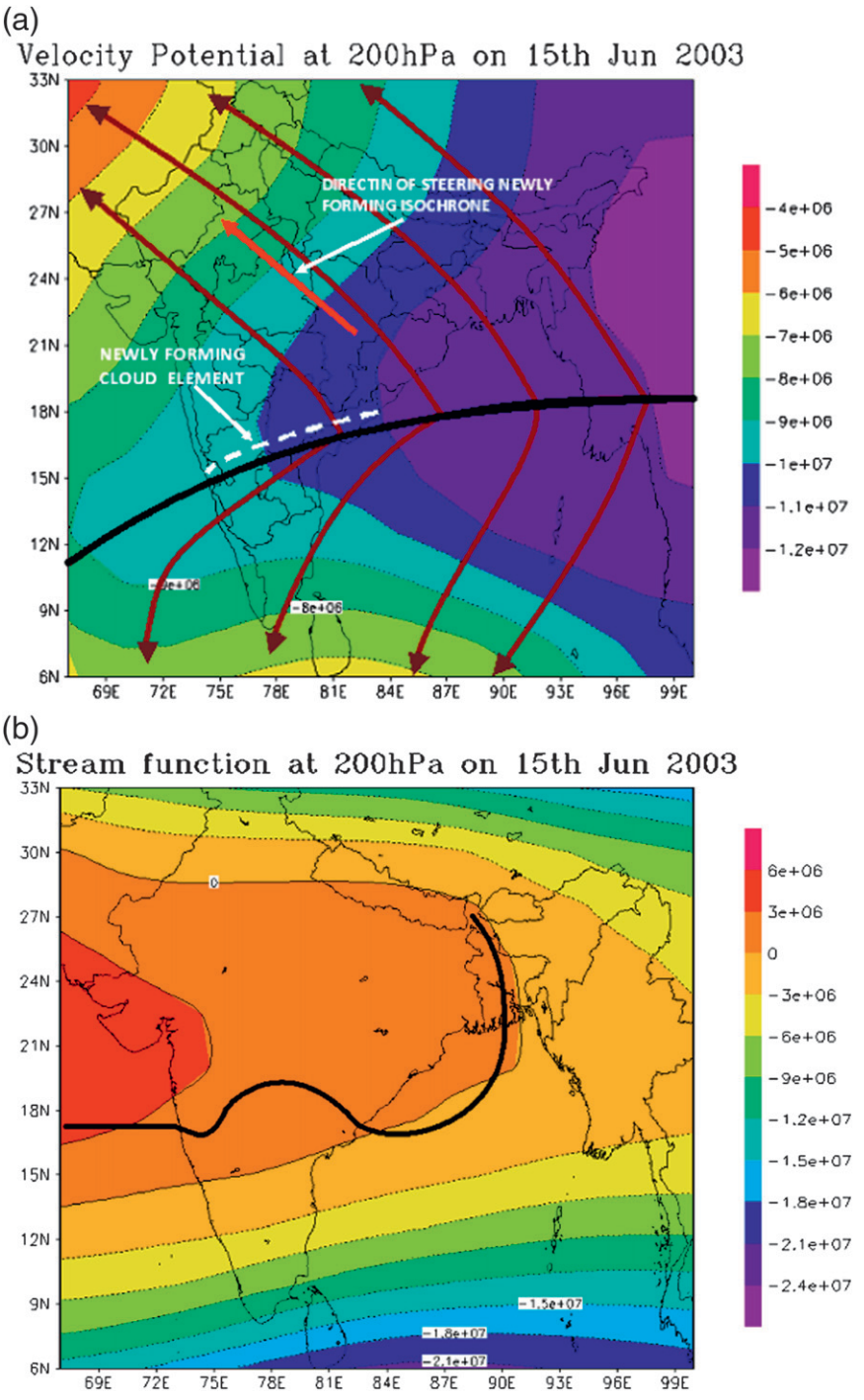

FIG. 14. (a) Velocity potential is shown as thin lines with shading. The divergent streamlines are indicated emanating from a line that lies close to the observed isochrone. Also marked are some salient features such as the direction of steering of the isochrone by the divergent wind. A dashed line shows where newly forming cloud elements ahead of the isochrone were noted from *CloudSat*. (b) The streamfunction (10^7 m^2 s^{-2}) at the 200-hPa level at 0000 UTC 15 Jun 2003 is shown by the solid and dashed lines. The thick black solid lines show the position of the onset isochrone for this date. (c) As in (a), but this is a forecast product from the mesoscale model for 15 Jun 2003.

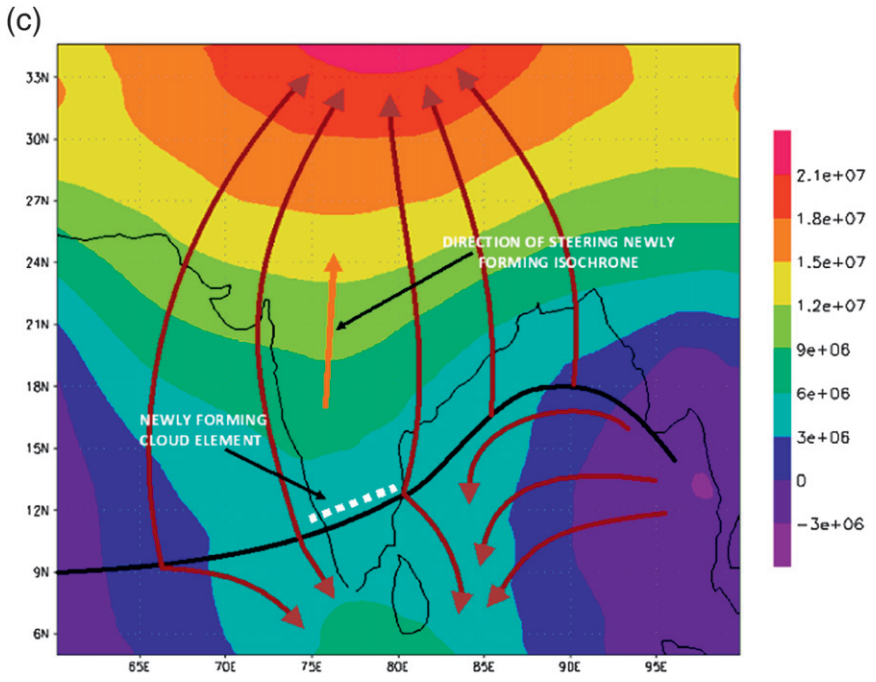

FIG. 14. (*Continued*)

the first 25 days of the meridional march that roughly covers a passage from Kerala at 7°N to New Delhi at 27°N. The title of the paper alludes to the first 25 forecast days. The number of days of progress of the monsoon from Kerala to New Delhi can vary, but on average it is around 25 days (based on the climatological positions of the onset isochrone as shown in Fig. 3). We show that this speed of northward motion is sensitive to the parameterization of the nonconvective rain and to the modeling of the soil moisture. We make use of a mesoscale model with a horizontal resolution of 25 km and 27 vertical levels that utilizes the initial states and lateral boundary conditions from the GFS/FNL NOAA model. All experiments cover the period 1–25 June for different years. The model internally carries algorithms for the nonconvective rains and the specification of soil moisture as discussed in this paper. A scenario for the meridional movement of the summer monsoon isochrones over India was developed based on satellite (*CloudSat*) and reanalysis datasets. That scenario suggested the following ingredients for the motion of the isochrones. There exists an interesting cloud, precipitation, and soil moisture asymmetry across the isochrones. The forward side, in the immediate vicinity of the isochrone, experiences light rains (partly anvil rains), increase of soil moisture, increase of buoyancy, and growth of newly developing clouds. This line of newly forming and growing clouds is steered to the north and eventually to the northwest by a divergent circulation that has its strongest upward motion along the parent isochrone. The rotational part of the wind has less of a role in the steering of the isochrone, since that flow generally appears to be parallel to the isochrone. The newly growing clouds slowly replace and become the parent isochrone. This process repeats itself during the isochrones' passage from Kerala to New Delhi. Scientifically this problem is important since the motion of the isochrones varies from year to year. Further study is warranted on possible strong variations of the rotational wind that can keep an isochrone stationary by having strong rotational winds oppose its meridional motion. The first runs, covering the seasons of the years 2000, 2002, and 2003, were designated as control experiments since they utilized the default values in the parameterization of the nonconvective rain and the soil moisture. These experiments clearly showed that forecasts based on the ARW-WRF carried slower speed for the meridional motion of the isochrones. This was followed up with a large number of model sensitivity experiments in which the intensity of nonconvective rains and soil moisture were increased by various percentages compared to the default values of the ARW-WRF. Through these sensitivity experiments it was clearly noted that a much improved motion of the model's summer monsoon onset isochrones from Kerala to New Delhi was

achievable, compared with the observed estimates of the India Meteorological Department. We have discussed those modifications for the parameterization of soil moisture and nonconvective rains in this study. Future modeling will require addressing this problem for operational weather forecasts. The mechanism portrayed here could well apply for the meridional motion of the ISO waves, where the higher-frequency motions could be affected by the divergent wind steering and the influences of soil moisture and stratiform clouds as shown here, and the low-frequency motions would form the envelope of such events. The mechanism portrayed here could also be used for the analysis and interpretation of the dry and wet spells of the monsoon. In future studies, it would also be important to examine specific years when unusual stagnation in the progress of monsoon isochrones has been noted. There have been times when stagnation was observed on more than one occasion in a given year and those are worth examining.

Acknowledgments. We wish to acknowledge the NASA Grant NNH09ZDA001N-PRECIP. DN gratefully acknowledges support from NSF CAREER ATM-0847472.

APPENDIX

On the Method of Computation of Isochrones

The same procedure is used for computing the position of the isochrones for both the observed and the predicted fields. IMD has adopted the following objective criteria for declaring monsoon onset over Kerala based on rainfall, wind field, and OLR data (http://www.imd.gov.in/section/nhac/dynamic/).

Their criteria are as follows: 1) Onset over Kerala is declared on the second day after 10 May; and 60% of the stations, from an available list of stations, report rainfall of 2.5 mm or higher for two consecutive days. 2) The depth of westerlies is maintained up to 600 hPa in a box between 0° and 10°N and 55°–80°E. The zonal wind speed at 925 hPa over the area bounded by 5°–10°N and 70°–80°E should be at least on the order of 15–20 kt (8–10 m s^{-1}). 4) INSAT-derived OLR value should be below 200 W m^{-2} in the box confined by 5°–10°N and 7°–75°E. For our analysis, after the onset of the monsoon over Kerala the onset isochrones for the later dates were drawn connecting the places that report rainfall of 2.5 mm or more for two consecutive days. If multiple lines are suggested by the above analysis, then the line closest to the previous 12-hourly position is used. For the observed state, we used these criteria to locate the position of the onset isochrone. This required examining the precipitation, winds, and OLR datasets. Our final observed positions, thus obtained, were very close to the official positions provided by IMD; they were not exactly the same since the datasets used were not identical. The above criteria also locate the isochrone locations over the ocean, especially the Bay of Bengal. For the same product derived from the output of the numerical model we use the same criteria. In the initial stages of the forecasts, to fill in the two consecutive days of rains in excess of 2.5 mm day^{-1} we use a mix of predicted products first and then we go back to observed rainfall estimates if needed. As the forecast proceeds beyond 2 days all datasets needed for locating the isochrone are provided by the forecast.

REFERENCES

Ananthakrishnan, R., V. Srinivasan, A. R. Ramakrishnan, and R. Jambunathan, 1968: Synoptic features associated with onset of southwest monsoon over Kerala. Forecasting Manual Rep. IV-18.2, India Meteorological Department, 17 pp.

Chang, C. P., 2005: The Maritime Continent monsoon. *The Global Monsoon System: Research and Forecast*. WMO/TD Rep. 1266, 156–178.

——, P. A. Harr, J. McBride, and H. H. Hsu, 2004: Maritime Continent monsoon. *East Asian Monsoon,* C. P. Chang, Ed., World Scientific Publishing, 107–150.

Chen, F., and Coauthors, 1996: Modeling of land surface evaporation by four schemes and comparison with FIFE observations. *J. Geophys. Res.,* **101,** 7251–7268.

——, R. Pielke Sr., and K. Mitchell, 2001: Development and application of land-surface models for mesoscale atmospheric models: Problems and promises. *Observation and Modeling of the Land Surface Hydrological Processes,* V. Lakshmi, J. Alberston, and J. Schaake, Eds., Amer. Geophys. Union, 107–135.

Derber, J. C., D. F. Parrish, and S. J. Lord, 1991: The new global operational analysis system at the National Meteorological Center. *Wea. Forecasting,* **6,** 538–547.

Dudhia, J., 1989: Numerical study of convection observed during the Winter Monsoon Experiment using a mesoscale two-dimensional model. *J. Atmos. Sci.,* **46,** 3077–3107.

Gill, A. E., 1980: Some simple solutions for heat-induced tropical circulation. *Quart. J. Roy. Meteor. Soc.,* **106,** 447–462.

Grell, G. A., 1993: Prognostic evaluation of assumptions used by cumulus parameterizations. *Mon. Wea. Rev.,* **121,** 764–787.

Hong, S.-Y., and J. J.-O. Lim, 2006: The WRF single-moment 6-class microphysics scheme (WSM6). *J. Kor. Meteor. Soc.,* **42,** 129–151.

——, J. Dudhia, and S.-H. Chen, 2004: A revised approach to ice microphysical processes for the bulk parameterization of clouds and precipitation. *Mon. Wea. Rev.,* **132,** 103–120.

Janjic, Z. I., 1994: The step-mountain eta coordinate model: Further developments of the convection, viscous sublayer, and turbulence closure schemes. *Mon. Wea. Rev.,* **122,** 927–945.

Janowiak, J. E., and P. Xie, 2003: A global-scale examination of monsoon-related precipitation. *J. Climate,* **16,** 4121–4133.

Kain, J. S., and J. M. Fritsch, 1993: Convective parameterization for mesoscale models: The Kain–Fritsch scheme. *The Representation of Cumulus Convection in Numerical Models, Meteor. Monogr.,* No. 46, Amer. Meteor. Soc., 165–170.

Kanamitsu, M., 1989: Description of the NMC Global Data Assimilation and Forecast System. *Wea. Forecasting,* **4,** 335–342.

Khole, M., A. B. Mazumdar, and S. Sunitha Devi, 2010: Onset, advance and withdrawal of southwest monsoon. *IMD Meteor. Monogr.,* No. 7/2010, India Meteorological Department, 1–13.

——, ——, ——, and B. P. Yadav, 2011: Onset, advance and withdrawal of southwest monsoon. *IMD Meteor. Monogr.,* No. 10/2011. India Meteorological Department, 1–20.

Krishnamurti, T. N., and R. Ramanathan, 1982: Sensitivity of the monsoon onset to differential heating. *J. Atmos. Sci.,* **39,** 1290–1306.

——, and L. Bounoua, 1996: *An Introduction to Numerical Weather Prediction Techniques*. CRC Press, 293 pp.

——, H. S. Bedi, V. M. Hardiker, and L. Ramaswamy, 2006: *An Introduction to Global Spectral Modeling*. Oxford University Press, 317 pp.

Li, L., and Coauthors, 2009: WindSat global soil moisture retrieval and validation. *IEEE Trans. Geosci. Remote Sens.,* **48,** 2224–2241, doi:10.1109/TGRS.2009.2037749.

Lwin, T., 2002: The climate changes over Myanmar during the last decades. *Water Resour. J.,* **212,** 95–106.

Mlawer, E. J., S. J. Taubman, P. D. Brown, M. J. Iacono and S. A. Clough 1997. Radiative transfer for inhomogeneous atmosphere: RRTM, a validated correlated-*k* model for the longwave. *J. Geophys. Res.,* **102,** 16 663–16 682.

Monin, A. S., and A. M. Obukhov, 1954: Basic laws of turbulent mixing in the surface layer of the atmosphere (in Russian). *Tr. Akad. Nauk SSSR Geofiz. Inst.,* **151,** 163–187.

Parrish, D. F., and J. C. Derber, 1992: The National Meteorological Center's spectral statistical interpolation analysis system. *Mon. Wea. Rev.,* **120,** 1747–1763.

Petersen, R. A., and J. D. Stackpole, 1989: Overview of the NMC production suite. *Wea. Forecasting,* **4,** 313–322.

Rao, Y. P., 1976. Southwest monsoon. *IMD Meteor. Monogr.,* No. 1/1976, India Meteorological Department, 107–185.

Skamarock, W. C., J. B. Klemp, J. Dudhia, D. O. Gill, D. M. Barker, W. Wang, and J. G. Powers, 2005. A description of the Advanced Research WRF version 2. NCAR Tech. Note NCAR/TN-468+STR, 88 pp.

Srivastava, A. K., and B. P. Yadav, 2009: Onset, advance and withdrawal of southwest monsoon. *IMD Meteor. Monogr.,* No. 7/2009, India Meteorological Department, 1–7.

Stano, G., T. N. Krishnamurti, T. S. V. Vijaya Kumar and A. Chakraborty, 2002: Hydrometeor structure of a composite monsoon depression using the TRMM radar. *Tellus,* **54A,** 370–381.

Wang, B., 2005: Theory. *Intraseasonal Variability of the Atmosphere–Ocean Climate,* K. M. Lau and D. E. Waliser, Eds., Springer, 315–317.

Yanai, M., C. Li, and Z. Song, 1992: Seasonal heating of the Tibetan Plateau and its effects on the evolution of the Asian summer monsoon. *J. Meteor. Soc. Japan,* **70,** 319–351.